

# Two-Dimensional Signal Detection Algorithm for Omni-Directional Signal Receiving Using Low-Frequency Orthogonal Magnetic Antenna

Shimin FENG, Shiyu WANG, Longfei WANG

Dept. of Electronic Engineering, Naval University of Engineering, PLA, Jiefang Street 117, 430033 Wuhan, China

fengshimin\_86@126.com, wangshiyuuestc@sina.com, 1105377726@qq.com

Submitted January 4, 2022 / Accepted May 23, 2022 / Online first May 23, 2022

**Abstract.** *This paper proposes a two-dimensional signal detection algorithm for low-frequency signal receiving using orthogonal magnetic antenna. According to the directional properties of a single antenna, the direction coefficient is introduced into the model. The algorithm based on Markov Chain Monte Carlo (MCMC) method can accurately estimate the direction coefficient and parameters of the noise in order to perform signal detection. The results show that the proposed algorithm is less affected by the direction of arrival and performs better, in terms of bit error rate, than that based on one-dimensional model. This study provides a valuable reference to omni-directional receiving of signals in low-frequency communication.*

## Keywords

Orthogonal antenna, omni-directional receiving, parameters estimation, non-Gaussian noise

## 1. Introduction

In the very-low-frequency (VLF) and ultra-low-frequency (ULF) communication, the noise shows obvious non-Gaussian characteristics due to the influence of atmospheric noise [1–5]. The bit error rate (BER) will seriously be reduced for signal detection and decoding when a traditional matched filter method is used. It was demonstrated that the method of channel parameters estimation based on accurate estimation of the noise parameters is the most accurate. The  $\alpha$ -stable distribution, mixed Gaussian distribution or class B noise model are often used for the modeling of atmospheric noise. In addition, the nonlinear regression estimation, spectral estimation and Markov chain Monte Carlo (MCMC) algorithm can be used in parameters estimation of the noise model for signal detection and decoding [3], [5–9]. It is important to mention that on account of the long wavelength in VLF and ULF communication, magnetic antennas, that have small size but high receiving efficiency, are usually used as receiving antennas in practice [10–15]. However, the radiation pattern of

a single magnetic antenna has blind frequency zones on the horizontal plane. Therefore, two antennas with orthogonal placement are usually used to form an omni-directional antenna for signal receiving [16–18]. There are two signals simultaneously received by the omni-directional antenna. In the study presented in [19–21], the stronger between the two signals can be selected for signal detection and decoding. In another method, the two signals can be synthesized into one signal by pre-signal processing, and the synthesized signal is then used for signal detection and decoding [19, 22, 23]. In the first method, only one signal is used and the signal strength may not necessarily be the maximum on account of the direction of arrival, which denotes a stronger signal but not the maximum signal-to-noise (SNR). In the second method, although the two signals are used, two noises are also synthesized, and the SNR of the synthesized signal containing noise also becomes worse. The BER of signal detection and decoding increases with the decrease of the SNR. Therefore, aiming at the characteristics of low-frequency orthogonal antenna, this paper directly uses the information of the two noisy signals, and extends the signal detection and decoding method based on channel noise parameter estimation in order to improve the BER performance.

## 2. The Omni-Directional Receiving Method of the Low-Frequency Orthogonal Antenna

The magnetic antenna is made up by multi-turn coils wound ferrite core. The coordinate system is established as shown in Fig. 1. The central axis of the loop plane of the antenna coils is the  $z$ -axis. Since the low-frequency antenna is an electrical small antenna, the current  $I$  at any point on the antenna conductor is considered to be evenly distributed. At any point  $r$  in space, the calculation formula of the electric field intensity and magnetic induction intensity of the antenna is shown in (1) [24], [25], where  $m = INA$ ,  $N$  denotes the number of coil turns of the magnetic antenna and  $A$  denotes the cross-sectional area of the magnetic antenna.

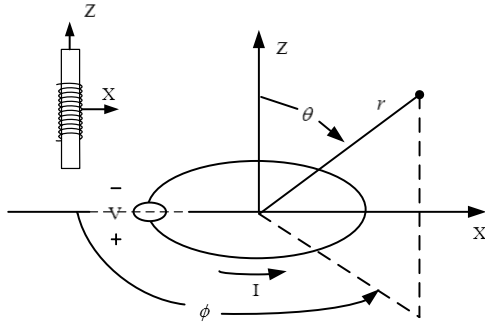


Fig. 1. Spherical coordinate system of the magnetic antenna.

$$\begin{cases} E_{\phi} = \frac{\zeta\beta^2 m}{4\pi r} \left(1 - \frac{j}{\beta r}\right) e^{-j\beta r} \sin\theta, \\ B_{\theta} = \frac{-\mu_0\beta^2 m}{4\pi r} \left(1 - \frac{j}{\beta r} - \frac{1}{\beta^2 r^2}\right) e^{-j\beta r} \sin\theta, \\ B_r = \frac{\mu_0\beta^2 m}{2\pi r} \left(\frac{j}{\beta r} + \frac{1}{\beta^2 r^2}\right) e^{-j\beta r} \cos\theta. \end{cases} \quad (1)$$

The radiated field of the magnetic antenna is a far field ( $\lim \beta r \rightarrow \infty$ ).  $E_{\phi}$  and  $B_{\theta}$  then play a dominant role:

$$\begin{cases} E_{\phi} = \frac{\zeta\beta^2 m}{4\pi r} e^{-j\beta r} \sin\theta, \\ B_{\theta} = \frac{-\mu_0\beta^2 m}{4\pi r} e^{-j\beta r} \sin\theta. \end{cases} \quad (2)$$

Equation (2) shows that  $E_{\phi}$  and  $B_{\theta}$  are proportional to  $\sin\theta$  [11, 20, 25]. The normalized direction function is given by:

$$F(\theta, \varphi) = \frac{f(\theta, \varphi)}{f_{\max}(\theta, \varphi)} = \frac{|B(\theta, \varphi)|}{|B_{\max}|} = |\sin\theta|. \quad (3)$$

Therefore, the radiation pattern of the magnetic antenna along the plane of the  $z$ -axis has an "8" shape, and blind frequency zones appear along the plane of the  $x$ -axis of the antenna. In order to avoid the blind frequency zones of a single antenna, an omni-directional antenna composed of two magnetic antennas in cross is used (cf. Fig. 2).

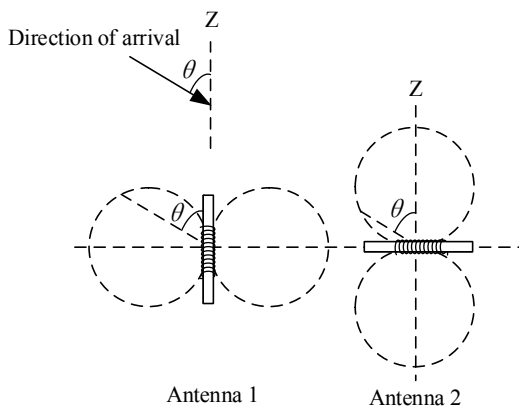


Fig. 2. Schematic diagram of the signal receiving process using the orthogonal magnetic antenna.

Assuming that the direction of arrival is  $\theta$ , and the maximum received signal with  $\theta = 0^\circ$  for Antenna 1 and  $\theta = 90^\circ$  for Antenna 2 is  $U\sin(\Omega t)$ , where  $\Omega$  is the frequency of the signal, the signal received by Antenna 1 is then  $U_1 = U\sin\theta \sin(\Omega t)$ , and the signal received by Antenna 2 is  $U_2 = U\cos\theta \sin(\Omega t)$ . Regardless of the value of  $\theta$ , at least one of the antennas can be guaranteed to receive the signal.

Two traditional signal detecting and decoding methods exist. The first one consists in selecting the antenna which has the stronger signal, as shown in Fig. 3(a). In the second method, one signal with its phase shifted by  $\pi/2$  is added to another, and the synthesized signal is then used for signal detecting and decoding, as shown in Fig. 3(b). The synthesized signal has nothing to do with the direction of arrival, which means the direction pattern on the horizontal plane has an "o" shape. As previously mentioned, the first method only uses one signal between the two antennas. Thus, it cannot be guaranteed that it is always the maximum when the direction of arrival changes. The second method uses the signals of two antennas, and the synthesized signal is always the maximum. However, because the pattern direction of the synthesized signal has an "o" shape, the received noise is  $\pi/2$  times that of a single antenna.

For these two methods of signal detection and decoding, the received signal model can be expressed as a one-dimensional sequence of signal and noise:

$$\mathbf{X}_i = \mathbf{S}_i + \mathbf{N}_i, \quad i = 1, 2, \dots, N. \quad (4)$$

There is no difference in signal detection and decoding between the two methods. However, they have a different BER performance leading to different SNR. These two methods are denoted by Algorithm 2 and Algorithm 3 in the comparison presented in the sequel. In this paper, a two-dimensional signal detection and decoding model (denoted by Algorithm 1) is proposed, in which the information of both signals are directly used. The schematic diagram of the proposed method is shown in Fig. 3(c).

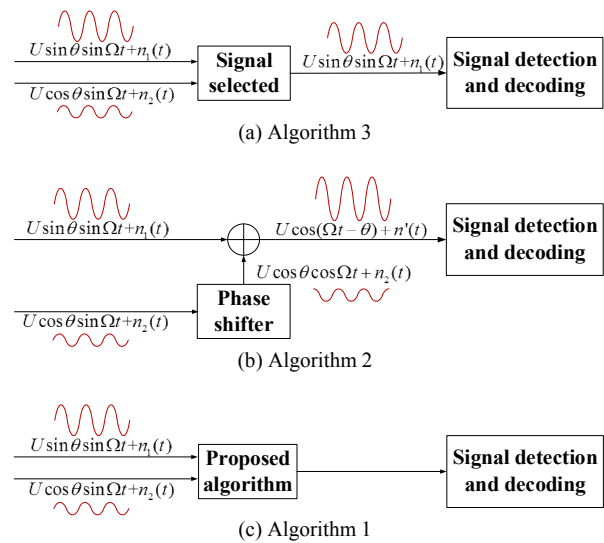


Fig. 3. Schematic diagram of signal detection and decoding for the orthogonal magnetic antenna.

### 3. Two-Dimensional Signal Detection and Decoding Model

A two-dimensional signal detection and decoding model is developed (cf. (5)). The following general assumptions are made: the signal detection or decoding is made on the baseband, and the code elements of the baseband signal are binary. Due to the fact that the communication rate is low in low-frequency communication, each symbol will be over-sampled. Since each antenna is directional, the two-dimensional signal detection and decoding model of the orthogonal antenna is established by introducing an extra direction coefficient vector  $\mathbf{f}(\theta)$ .

$$\mathbf{X}_i = \mathbf{f}(\theta) \otimes \mathbf{S}_i + \mathbf{N}_i, \quad i = 1, 2, \dots, N \quad (5)$$

where  $\mathbf{S}_i$  represents the noiseless signals,  $\mathbf{N}_i$  denotes the additive and two-dimensional noise sequence, and  $\mathbf{X}_i$  represents the received noisy signals.

Assuming that the over-sampling rate of each symbol is  $M$ , which indicates that each symbol will be sampled  $M$  times, then  $\mathbf{S}_i = [s_{i1}, \dots, s_{iM}]$ ,  $\mathbf{X}_i = [\mathbf{x}_{i1}, \dots, \mathbf{x}_{iM}]$ ,  $\mathbf{N}_i = [\mathbf{n}_{i1}, \dots, \mathbf{n}_{iM}]$ ,  $s_{ij} \in \{1, -1\}$ ,  $i = 1, \dots, N$ ,  $j = 1, \dots, M$ ,  $\mathbf{x}_{ij} = [x_{ij}^1, x_{ij}^2]^T$  are the signals received by the two antennas, respectively.  $\mathbf{n}_{ij} = [n_{ij}^1, n_{ij}^2]^T$  are the noises received by the two antennas, respectively. The vector function  $\mathbf{f}: \mathbb{R} \rightarrow \mathbb{R}^2$  is  $[\sin\theta; \cos\theta]^T$ , such that  $\theta \in [0, \pi/2]$ , which denotes the direction coefficients of the two antennas.

In the VLF and ULF bands, a two-dimensional non-Gaussian noise model is used:

$$\mathbf{n}_{ij} \stackrel{\text{dist}}{=} \sum_{l=1}^k \omega_l N(\mathbf{0}, \Sigma_l) \quad (6)$$

where  $\stackrel{\text{dist}}{=}$  represents the same distribution,  $N(\mathbf{0}, \Sigma_l)$  denotes the  $l^{\text{th}}$  two-dimensional Gaussian distribution with a mean of  $\mathbf{0}$  and a covariance matrix  $\Sigma_l$ ,  $\Sigma_l = [\sigma_1^2, \rho\sigma_1\sigma_2; \rho\sigma_2\sigma_1; \sigma_2^2]$ ,  $\rho$  denotes the correlation coefficient of the received noise of the two magnetic antennas, and  $\omega_l$  is the weight of the  $l^{\text{th}}$  two-dimensional Gaussian distribution satisfying  $\sum_{l=1}^k \omega_l = 1$ .

For the noise sequence  $\{\mathbf{n}_{ij}\}$ , the index variable  $\mathbf{T} = \{t_{ij}\}$  is introduced to sort  $\mathbf{n}_{ij}$ . When  $\mathbf{n}_{ij}$  belongs to the  $l^{\text{th}}$  two-dimensional Gaussian distribution, the value of  $t_{ij}$  is equal to  $l$ , and  $t_{ij}$  satisfies:

$$p(t_{ij} = l) = \omega_l, \quad l = 1, 2, \dots, k. \quad (7)$$

According to (6) and (7), the equivalent expression of the noise sequence can be derived:

$$\mathbf{n}_{ij} \sim N(\mathbf{0}, \Sigma_l), \quad t_{ij} = l. \quad (8)$$

Therefore, according to (5) and (8), the two-dimensional signal detection and decoding model can be finally expressed as:

$$\mathbf{x}_{ij} \sim N(\mathbf{f}(\theta) \cdot s_{ij}, \Sigma_l), \quad t_{ij} = l. \quad (9)$$

### 4. MCMC Signal Detection Algorithm

Based on the Bayesian theory, the unknown parameters can be accurately estimated using an MCMC algorithm according to the posterior distribution, which can be derived from the current information and the prior distribution [7, 8, 26]. In the signal detection model,  $\mathbf{X}$  is the received signal considered as the known current information.  $\{\mathbf{f}(\theta), \Sigma_l, \omega, \mathbf{T}, \mathbf{S}\}$  are the parameters that need to be estimated. The posterior distribution of  $\{\mathbf{f}(\theta), \Sigma_l, \omega, \mathbf{T}, \mathbf{S}\}$  satisfies:

$$P(\mathbf{f}(\theta), \Sigma_l, \omega, \mathbf{T}, \mathbf{S} | \mathbf{X}) \propto P(\mathbf{X} | \mathbf{f}(\theta), \Sigma_l, \omega, \mathbf{T}, \mathbf{S}) \cdot P(\mathbf{f}(\theta), \Sigma_l, \omega, \mathbf{T}, \mathbf{S}). \quad (10)$$

When selecting the prior distribution of each parameter, the conjugate prior distribution should be selected as far as possible in order to ensure that the posterior distribution of the parameters belongs to the same distribution family as the prior distribution. Afterwards, by deriving the posterior distribution ahead of schedule, the implementation of the MCMC algorithm will have a concise form and higher efficiency. The conjugate prior distributions of each parameter are shown in Tab. 1.

| Parameter            | Conjugate prior distribution          | Denotes  |
|----------------------|---------------------------------------|--|
| $\mathbf{f}(\theta)$ | Two-dimensional Gaussian distribution | $\mathbf{f}(\theta) \sim N(\boldsymbol{\mu}, \boldsymbol{\Psi})$ |
| $\Sigma_l$           | Inverse Wishart distribution          | $\Sigma_l \sim W^{-1}(m_l, \Lambda_l^{-1})$                      |
| $\omega$             | Dirichlet distribution                | $\omega \sim D(\eta, \dots, \eta)$                               |

Tab. 1. Conjugate prior distributions of the parameters.

In a time window, the two-dimensional signal received by an orthogonal antenna is  $\mathbf{X}$ .

1. **Setting prior information** :  $\boldsymbol{\mu}, \boldsymbol{\Psi}, m_l, \Lambda_l, b, \eta$
2. **Initializing parameters** :  $\mathbf{a}, \Sigma_l, \mathbf{S}, \omega, \mathbf{T}$
3. **for**  $c = 1 : z$  **do**
4. Draw a new sample and update  $\mathbf{T}$  from posterior distribution of  $\mathbf{T}$
5. Draw a new sample and update  $\omega$  from posterior distribution of  $\omega$
6. Draw a new sample and update  $\mathbf{f}(\theta)$  from posterior distribution of  $\mathbf{f}(\theta)$
7. Draw a new sample and update  $\Sigma_l$  from posterior distribution of  $\Sigma_l$
8. Draw a new sample and update  $\mathbf{S}$  from posterior distribution of  $\mathbf{S}$
9. **end for**
10. **Parameters estimation** : calculate the means of obtained sample  $\mathbf{f}(\theta), \Sigma_l, \omega, \mathbf{T}$  respectively from  $c = Z' \textcircled{1}$  to  $c = Z$  as the estimations of  $\mathbf{f}(\theta), \Sigma_l, \omega, \mathbf{T}$
11. **Signal detection and decoding**: calculate the probability of the signal as 1 and -1 according to the estimations of parameters and  $\mathbf{X}$ , and judge by the Gibbs sampler

<sup>①</sup> Iterations when all parameters are convergent

Fig. 4. Signal detection and decoding algorithm.

For  $S_i$ , if every symbol occurs with equal probability, its prior distribution is given by:

$$P(S_i = 1) = P(S_i = -1) = \frac{1}{b} = \frac{1}{2} \quad (11)$$

where  $\boldsymbol{\mu}, \boldsymbol{\Psi}, m_l, \boldsymbol{\Lambda}_l, \eta, b$  are prior information.

If  $\mathbf{E} = \{\mathbf{f}(\theta), \boldsymbol{\Sigma}_l\}$  and the parameters in  $\mathbf{E}$  are denoted by  $\boldsymbol{\varphi} = \{\boldsymbol{\mu}, \boldsymbol{\Psi}, m_l, \boldsymbol{\Lambda}_l\}$ , then equation (10) can be extended as:

$$\begin{aligned} P(\mathbf{E}, \boldsymbol{\varphi}, \boldsymbol{\omega}, \mathbf{T}, \mathbf{S}, b, \eta | \mathbf{X}) &\propto P(\mathbf{X} | \mathbf{E}, \mathbf{T}) P(\mathbf{T} | \boldsymbol{\omega}) \\ &\cdot P(\boldsymbol{\omega} | \eta) P(\mathbf{E} | \boldsymbol{\varphi}) P(\mathbf{S} | b) \\ &\cdot P(\boldsymbol{\varphi}) P(\eta) P(b). \end{aligned} \quad (12)$$

The signal detection and decoding algorithm is detailed in Fig. 4.

In the iterations, the parameters are drawn and updated as follows:

(1) Draw a new sample and update index variable  $\mathbf{T}$ :

The posterior distribution of  $t_{ij}$  is given by:

$$P(t_{ij} = l | \dots) \propto \omega_l N(\mathbf{x}_{ij}; \mathbf{f}(\theta) \cdot s_{ij}, \boldsymbol{\Sigma}_l). \quad (13)$$

The posterior probability can be first calculated by (13), then  $t_{ij}$  can be updated by the Gibbs sampler, which determines the located range of  $P(t_{ij} = l | \dots)$  according to a random number generated from the uniform distribution of  $U(0,1)$ . The number of  $t_{ij} = l$  can then be counted as  $n_l$ .

(2) Draw a new sample and update parameter  $\boldsymbol{\omega}$ :

The posterior probability distribution of  $\boldsymbol{\omega}$  is a new Dirichlet distribution:

$$\boldsymbol{\omega} | \dots \sim D(\eta + n_1, \eta + n_2, \dots, \eta + n_l) \quad (14)$$

where  $n_l$  is the number of measurements which belongs to the two-dimensional Gaussian distribution  $N(\mathbf{0}, \boldsymbol{\Sigma}_l)$ , and  $\boldsymbol{\omega}$  can be updated by the Gibbs sampler, in which a random number is generated from the Dirichlet distribution with the form expressed in (14).

(3) Draw a new sample and update parameter  $\mathbf{f}(\theta)$ :

The posterior probability distribution of  $\mathbf{f}(\theta)$  is a new two-dimensional Gaussian distribution:

$$\mathbf{f}(\theta) | \dots \sim N(\mathbf{H}, \mathbf{K}) \quad (15)$$

where:

$$\mathbf{H} = \mathbf{K} \left( \boldsymbol{\Psi}^{-1} \boldsymbol{\mu} + \boldsymbol{\Sigma}_l^{-1} \sum_{i=1}^N \sum_{j=1, t_{ij}=l}^M s_{ij} \mathbf{x}_{ij} \right), \quad (16)$$

$$\mathbf{K} = \left( \boldsymbol{\Psi}^{-1} + \boldsymbol{\Sigma}_l^{-1} \sum_{i=1}^N \sum_{j=1, t_{ij}=l}^M s_{ij}^2 \right)^{-1}. \quad (17)$$

According to Gibbs sampler,  $\mathbf{f}(\theta)$  can be sampled and updated from the new two-dimensional Gaussian distribution with the form expressed in (15).

(4) Draw a new sample and update parameter  $\boldsymbol{\Sigma}_l$ :

The posterior probability distribution of  $\mathbf{f}(\theta)$  is a new inverse Wishart distribution:

$$\sigma_l^{-2} | \dots \sim W^{-1}(m_l + n_l, \mathbf{A}) \quad (18)$$

where:

$$\mathbf{A} = \sum_{i=1}^N \sum_{j=1, t_{ij}=l}^M \text{tr}(\mathbf{P}) \mathbf{P}^T + \boldsymbol{\Lambda}^{-1}, \quad (19)$$

$$\mathbf{P} = \mathbf{x}_{ij} - \mathbf{f}(\theta) \cdot s_{ij}. \quad (20)$$

According to Gibbs sampler,  $\boldsymbol{\Sigma}_l$  can be sampled and updated from the new inverse Wishart distribution with the form expressed in (18).

(5) Make judge and update  $S_i$ :

The posterior probability distribution of  $S_i$  is given by:

$$P(S_i = -1 | \dots) = \prod_{j=1, t_{ij}=l}^M \frac{1}{2\pi |\boldsymbol{\Sigma}_l|^{\frac{1}{2}}} \exp(\mathbf{G}) P(S_i = -1), \quad (21)$$

$$P(S_i = 1 | \dots) = \prod_{j=1, t_{ij}=l}^M \frac{1}{2\pi |\boldsymbol{\Sigma}_l|^{\frac{1}{2}}} \exp(\mathbf{G}) P(S_i = 1) \quad (22)$$

where:

$\mathbf{1} = [1, 1, \dots, 1]$  is a  $1 \times M$  sequence,  $\mathbf{G} = -\mathbf{B}_2^T \boldsymbol{\Sigma}_l^{-1} \mathbf{B}_2 / 2$ ,  $\mathbf{B}_1 = \mathbf{x}_{ij} + \mathbf{f}(\theta) \cdot s_{ij}$ , and  $\mathbf{B}_2 = \mathbf{x}_{ij} - \mathbf{f}(\theta) \cdot s_{ij}$ .

The posterior probability can be first calculated by (21) and (22).  $S_i$  can then be judged and updated by the Gibbs sampler, which is determined by a random number generated from the uniform distribution of  $U(0,1)$ .

In order to test the performance of the algorithm, a testing platform is built (cf. Fig. 5). The testing system mainly includes an omni-directional magnetic antenna, a pattern synthesis equipment, a multichannel receiver, a ESRP3 EMI test receiver and a receiving terminal. The omni-directional magnetic antenna is used to receive the VLF signal which is transmitted far from 25 km away. The two VLF signals are first processed by the pattern synthesis equipment that can output three kinds of signals: signal of Antenna 1, signal of Antenna 2 and signal with radiation pattern having an "o" shape. All the signals are downconverted to baseband in the multichannel receiver, then stored, demodulated and decoded in the receiving terminal, in which the algorithms are embedded. In the test process, the direction of the omni-directional magnetic antenna is rotated on a horizontal plane in order to form different directions of arrival. The radiation power is adjusted to control different SNR, which can be simultaneously observed

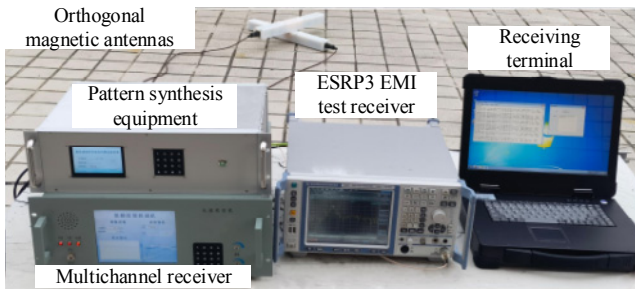


Fig. 5. Orthogonal magnetic antennas receiving testing system.

on the EMI test receiver. The packet data decoded in the receiving terminal is compared with the transmitted signal, and it is used for the BER analysis.

## 5. Results and Analysis

### 5.1 Noise Parameter Estimation

In order to verify the applicability of the model, the proposed algorithm is first used to estimate the actual received noise of the two antennas. Very-low-frequency and ultra-low-frequency noise present obvious non-Gaussian characteristics, as shown in Fig. 6. When  $k = 2$  in the two-dimensional Gaussian mixture noise model, the noise parameters estimated by the proposed algorithm are  $\omega = [0.977; 0.023]$ ,  $\Sigma_1 = [6.429 \ 1.65; 1.65 \ 6.268]$  and  $\Sigma_2 = [414.346 \ 401.799; 401.799 \ 580.689]$ .

For the estimated noise parameters,  $\Sigma_1$  represents the Gaussian part with a large proportion in the noise. When the electrical parameters of the two antennas are mainly the same, the noise power of this part is also the same, and the correlation coefficient is 0.26.  $\Sigma_2$  represents the non-Gaussian part of the noise with a small proportion, and the noise power of this part has a small difference, with a correlation coefficient of 0.82. The results are accorded with the

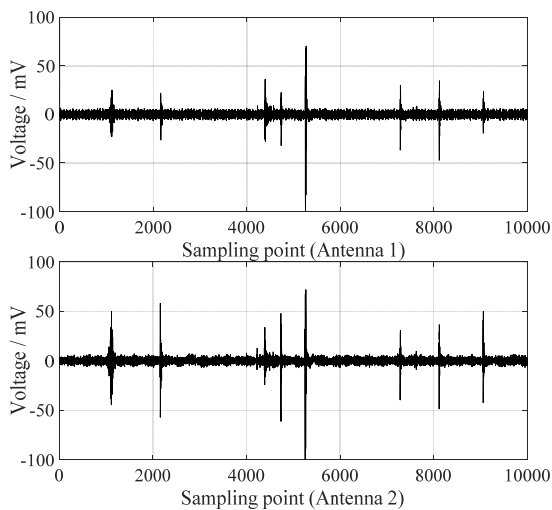


Fig. 6. Actual noise received by the low-frequency orthogonal magnetic antennas.

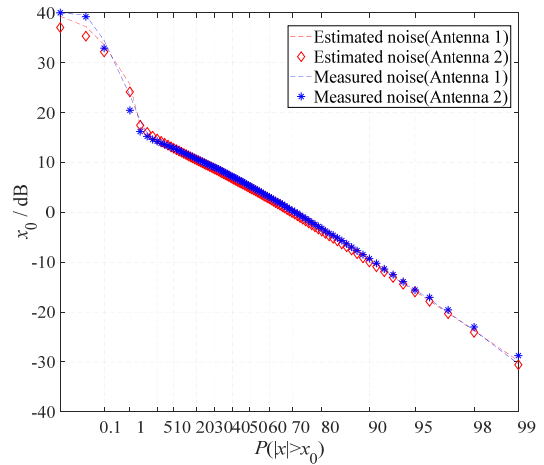


Fig. 7. Amplitude probability distribution of the measured noise compared with the estimated noise.

actual situation. The part of Gaussian noise comes from the impedance of the antennas and amplifier circuits which is not correlated, as well as the Gaussian noise received from the environments, which is correlated due to the fact that the receiving areas of the two antennas are not independent. In general, the correlation coefficient of the Gaussian noise is small. The non-Gaussian noise mainly comes from atmospheric noise caused by lightning, which is correlated, and therefore the correlation coefficient is large.

A comparison between the amplitude probability distribution (APD) of the measured noise and the estimated noise is shown in Fig. 7. It can be seen that the APD of the noise estimated by the proposed algorithm is almost identical to the measured noise, with a slight error within the area of  $P < 1\%$ .

### 5.2 BER Analysis

Because the direction of arrival  $\theta$  varies, it affects the information received by the two antennas. Therefore, the influence of the value of  $\theta$  on the BER of the proposed algorithm is analyzed. The BER curve is shown in Fig. 8.

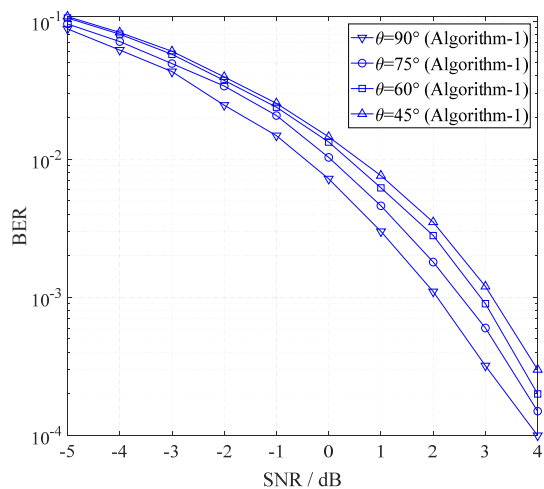
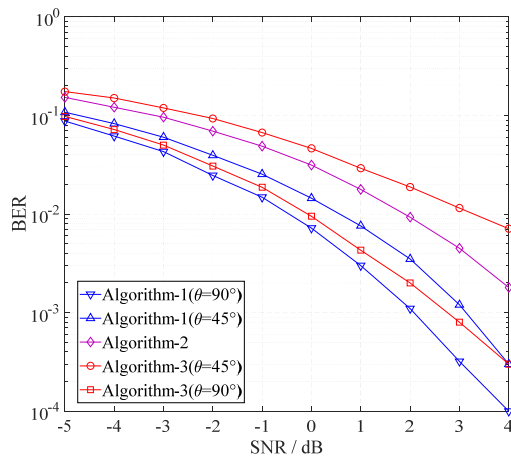


Fig. 8. BER for different values of angle  $\theta$ .



**Fig. 9.** BER of the proposed algorithm compared with the traditional algorithms.

It can be seen that the BER is related to the direction of arrival. When the direction of arrival is smaller or larger ( $\theta = 90^\circ$ , which is similar to  $\theta = 0^\circ$ ), the BER of signal detection and decoding is lower. When the direction of arrival for the two antennas is the same ( $\theta = 45^\circ$ ), the BER is the highest. From the perspective of information theory, when  $\theta$  is larger or smaller, the difference between the information received by the two antennas is larger, which means the entropy is larger, and therefore the BER is lower. When  $\theta = 45^\circ$ , the information received by the two antennas are similar, which indicates that the entropy is the smallest, and therefore the BER is the highest.

The BER of the proposed algorithm is compared with those of the other two algorithms (cf. Fig. 9). The BERs of Algorithm 1 and Algorithm 3 are affected by the direction of arrival. Thus, Figure 9 shows the maximum BER ( $\theta = 45^\circ$ ) and minimum BER ( $\theta = 90^\circ$ ) of Algorithm 1 and Algorithm 3. It can be deduced from Fig. 9 that:

(1) Regardless of the value of  $\theta$ , the BER of Algorithm 1 is lower than that of Algorithm 2;

(2) For the same value of  $\theta$ , the BER of Algorithm 1 is lower than that of Algorithm 3.

(3) The BER of Algorithm 1 is less affected by the value of  $\theta$  than that of Algorithm 3. In addition, the BER is close to the minimum BER of Algorithm 3 with a small difference;

(4) As the SNR increases, the maximum BER of Algorithm 1 approaches the minimum BER of Algorithm 3. When the SNR is greater than or equal to 4 dB, the maximum BER of Algorithm 1 is coherent with the minimum BER of Algorithm 3.

## 6. Conclusion

In the process of low-frequency signal receiving using orthogonal antennas, the signal detection and judgment based on a two-dimensional model is efficient. Compared with the traditional method based on one-dimensional

model, the proposed algorithm has the following advantages: (1) The BER of the proposed algorithm is less affected by the direction of arrival; (2) Under the same receiving conditions, the BER performance can be efficiently improved. Therefore, a higher SNR and a greater improvement can be obtained. The algorithm can also be easily implemented using simple hardware equipment. It has high reference value for the omni-directional receiving of signals in low-frequency communication.

## Acknowledgments

This thesis is supported by the National Natural Science Foundation of China (no. 41774021).

## References

- [1] ABRAHAM, D. A. Detection-threshold approximation for non-Gaussian backgrounds. *IEEE Journal of Oceanic Engineering*, 2010, vol. 35, no. 2, p. 355–365. DOI: 10.1109/JOE.2010.2043752
- [2] SCHLEGEL, C., MALLAY, M., TOUESNARD, C. Atmospheric magnetic noise measurements in urban areas. *IEEE Magnetics Letters*, 2014, vol. 5, p. 1–4. DOI: 10.1109/LMAG.2014.2330337
- [3] MCDONALD, K. F., BLUM, R. S. A statistical and physical mechanisms-based interference and noise model for array observations. *IEEE Transactions on Signal Processing*, 2000, vol. 48, no. 7, p. 2044–2056. DOI: 10.1109/78.847789
- [4] GASDIA, F., MARSHALL, R. A. Assimilating VLF transmitter observations with an LETKF for spatial estimates of the D-region ionosphere. *IEEE Transactions on Geoscience and Remote Sensing*, 2020, vol. 58, no. 5, p. 3526–3543. DOI: 10.1109/TGRS.2019.2957716
- [5] CHEN, Q. D., LIU, R., LIU, Y., et al. LF/VLF electromagnetic pulse measurement system. *Chinese Journal of Radio Science*, 2020, vol. 35, no. 5, p. 791–798. (In Chinese) DOI: 10.13443/j.cjors.2019092001
- [6] GU, X., LI, G., PANG, H., et al. Statistical analysis of very low frequency atmospheric noise caused by the global lightning using ground-based observations in China. *Journal of Geophysical Research: Space Physics*, 2021, vol. 126, no. 6, p. 1–11. DOI: 10.1029/2020JA029101
- [7] LOMBARDI, M. J. Bayesian inference for alpha-stable distribution: A random walk MCMC approach. *Computation Statistics & Data Analysis*, 2007, vol. 51, no. 5, p. 2688–2700. DOI: 10.1016/j.csda.2006.01.009
- [8] YING, W. W., JIANG, Y. Z., LIU, Y. L. Parameters estimation for mixture model of atmospheric noise through MCMC method. *Systems Engineering Electronics*, 2012, vol. 34, no. 6, p. 1241–1245. (In Chinese) DOI: 10.3969/j.issn.1001-506X.2012.06.29
- [9] YING, W. W., JIANG, Y. Z., LIU, Y. L. A blind receiver with multiple antennas in impulsive noise modeled as the sub-Gaussian distribution via the MCMC algorithm. *IEEE Transactions on Vehicular Technology*, 2013, vol. 62, no. 7, p. 3492–3497. DOI: 10.1109/TVT.2013.2250535
- [10] WEISS, E., ALIMI, R. *Low-Power and High-Sensitivity Magnetic Sensors and Systems*. London (UK): Artech House, 2018. ISBN: 9781630812430
- [11] RIPKA, P. (Ed.). *Magnetic Sensors and Magnetometers*. London (UK): Artech House, 2021. ISBN: 9781630817428

- [12] FÜLLEKRUG, M., MEZENTSEV, A., WATSON, R., et al. Array analysis of electromagnetic radiation from radio transmitters for submarine communication. *Geophysical Research Letters*, 2014, vol. 41, no. 24, p. 9143–9149. DOI: 10.1002/2014GL062126
- [13] GHAFFAR, A., AWAN, W. A., ZAIDI, A., et al. Compact ultra wide-band and tri-band antenna for portable device. *Radioengineering*, 2020, vol. 29, no. 4, p. 601–608. DOI: 10.13164/re.2020.0601
- [14] ZAIDI, A., AWAN, W. A., HUSSAIN, N., et al. A wide and tri-band flexible antennas with independently controllable notch bands for sub-6-GHz communication system. *Radioengineering*, 2020, vol. 29, no. 1, p. 44–51. DOI: 10.13164/re.2020.0044
- [15] AWAN, W. A., ALIBAKHSHIKENARI, M., LIMITI, E. A polydimethyl-siloxane based conformal ultra-wideband antenna with additional GSM band. In *2021 IEEE Asia-Pacific Microwave Conference (APMC)*. Brisbane (Australia), 2021, p. 67–69. DOI: 10.1109/APMC52720.2021.9661872
- [16] KHALID, H., AWAN, W. A., HUSSAIN, M., et al. Design of an integrated sub-6 GHz and mmwave MIMO antenna for 5G handheld devices. *Applied Sciences*, 2021, vol. 11, no. 18, p. 1–21. DOI: 10.3390/app11188331
- [17] ZAHRA, H., AWAN, W. A., ALI, W., et al. A 28 GHz broadband helical inspired end-fire antenna and its MIMO configuration for 5G pattern diversity applications. *Electronics*, 2021, vol. 10, no. 4, p. 1–15. DOI: 10.3390/electronics10040405
- [18] HUSSAIN, N., AWAN, W. A., ALI, W., et al. Compact wideband patch antenna and its MIMO configuration for 28 GHz applications. *AEU-International Journal of Electronics and Communications*, 2021, vol. 132, p. 1–8. DOI: 10.1016/j.aeue.2021.153612
- [19] SHI, W., LI, G. M., QIN, J. P. A method for directional receiving of VLF signals with magnetic antennas. In *ICWMMN 2013-5th IET International Conference on Wireless, Mobile & Multimedia Networks*. Beijing (China), 2013, p. 51–54. DOI: 10.1049/cp.2013.2376
- [20] KHAN, M. A., SUN, J., LI, B. D., et al. Magnetic sensors—A review and recent technologies. *Engineering Research Express*, 2021, vol. 3, no. 2, p. 1–22. DOI: 10.1088/2631-8695/ac0838
- [21] WEI, S., LIAO, X., ZHANG, H., et al. Recent progress of fluxgate magnetic sensors: Basic research and application. *Sensors*, 2021, vol. 21, no. 4, p. 1–18. DOI: 10.3390/s21041500
- [22] GUO, H. B. The research and realization of active omni directional small loops antenna loaded ferrite core. Harbin: Harbin Engineering University, 2007. (In Chinese) DOI: 10.7666/d.y1097838
- [23] FU, T. H., SU, M. Research on long wave communication technique for UUV. *Journal of Sichuan Ordnance*, 2013, vol. 34, no. 3, p. 83–85. (In Chinese) DOI: 10.11809/scbgxb2013.03.024
- [24] XIE, C. F., RAO, K. J., ZHAO, J. S. *Electromagnetic Fields and Waves*. 5<sup>th</sup> ed. Beijing (China): Higher Education Press, 2019. (In Chinese) ISBN: 9787040525182
- [25] SONG, Z., ZHANG, J. H., HUANG, Z. *Antenna and Propagation*. 3<sup>rd</sup> ed. Xi'an (China): Xidian University Publishing House, 2016. (In Chinese) ISBN: 9787560640563
- [26] ROBERT, C. P., ELVIRA, V., TAWN, N., et al. Accelerating MCMC algorithms. *Wiley Interdisciplinary Reviews: Computational Statistics*, 2018, vol. 10, no. 5, p. 1–14. DOI: 10.1002/wics.1435

## About the Authors ...

**Shimin FENG** was born in Hebei Province, China in 1986. He received the Ph.D. degrees from the Naval University of Engineering in 2015. His research interests include receiving antenna design and signal processing technology in low-frequency wireless communications.

**Shiyu WANG** (corresponding author: wangshiyuuestc@sina.com, College of Electronic Engineering, Naval University of Engineering, Wuhan, Hubei 430033, China) was born in Shandong Province, China in 1996. He received a Master degree from the Naval University of Engineering in 2020. His research interests include wireless communications.

**Longfei WANG** was born in Shandong Province, China in 1998. He received a Bachelor degree from the Ocean University of China in 2019, with a research field of wireless communication. His research interests include wireless communications.